Applied Surface Science 393 (2017) 103–109

Contents lists available at ScienceDirect

Applied Surface Science

journal homepage: www.elsevier.com/locate/apsusc

Full Length Article

Surface energy effects on the stability of anatase and rutile nanocrystals: A predictive diagram for Nb_2O_5-doped-TiO_2

Andre Luiz da Silva [a], Dachamir Hotza [a], Ricardo H.R. Castro [b,*]

[a] Department of Chemical Engineering (EQA), Graduate Program on Materials Science and Engineering (PGMAT), Federal University of Santa Catarina (UFSC), 88040-900 Florianópolis, SC, Brazil
[b] Department of Materials Science & Engineering and NEAT ORU, University of California, Davis, One Shields Avenue, Davis, CA 95616, United States

ARTICLE INFO

Article history:
Received 26 August 2016
Received in revised form
22 September 2016
Accepted 25 September 2016
Available online 26 September 2016

Keywords:
Titanium dioxide
Anatase
Rutile
Surface energy
Enthalpy
Phase diagram
Nanoparticles

ABSTRACT

Titanium dioxide nanoparticles are widely used for photocatalysis, and the relative fraction of titanium dioxide polymorph, i.e. anatase, rutile, or brookite, significantly affects the final performance. Even though conventional phase diagrams indicate a higher stability for the rutile polymorph, it is well established that nanosizes benefit the anatase phase due to its smaller surface energy. However, doping elements are expected to change this behavior, once changes in both surface and bulk energies may occur. Nb_2O_5 is commonly added to TiO_2 to allow property control. However, the effect of niobium on the relative stability of anatase and rutile phases is not well understood from the thermodynamic point of view. The objective of this work was to build a new predictive nanoscale phase diagram for Nb_2O_5-doped TiO_2. Water adsorption microcalorimetry and high temperature oxide melt solution were used to obtain the surface and bulk enthalpies. The phase diagram obtained shows the stable titania polymorph as a function of the composition and size.

1. Introduction

Titanium dioxide presents three main polymorphs: anatase, rutile and brookite. All three polymorphs can be readily synthesized in the laboratory and typically, the metastable anatase and brookite will transform into the thermodynamically stable rutile upon calcination at temperatures exceeding 600 °C [1]. Some studies have been performed on the thermodynamic viewpoint to better understand the stability of the TiO_2 polymorphs [2–7]. Even though rutile is the most stable form of TiO_2 and anatase is known as a metastable phase, at the nanoscale, anatase becomes more stable than rutile [2,8]. This is related to the competition between surface and bulk energies, leading to a crossover in thermodynamic stability when particle sizes are decreased. Anatase thus shows a range of particle sizes in which it is thermodynamically stable as long as coarsening is avoided [2].

Several dopants have been studied targeting the control of TiO_2 stability at the nanoscale and its properties. Among them, niobium improves TiO_2 performance for oxygen sensing [9–11], solar cells applications [12,13], and photocatalysis [14–16]. When doping TiO_2 with Nb_2O_5, since the ionic radius of Nb^{5+} (0.64 Å) is only slightly larger than Ti^{4+} (0.605 Å), Nb^{5+} forms solid solution in the lattice of TiO_2. One Ti cationic vacancy is then created per every four Nb ions to compensate the excess charge, or a stoichiometric reduction of Ti^{4+} to Ti^{3+} can take place to accommodate it [17]. Atanacio *et al.* [18] have showed that niobium has a potential to segregate on the surface of TiO_2 under oxidizing conditions. The segregation tendency is enhanced by the presence of titanium vacancies, which are formed at the TiO_2/O_2 interface and trapped at the surface.

The use of dopants prone to segregation has been cited as a tool to decrease interface energies in oxides [19–24] and observed to follow Eq. (1):

$$\gamma_s = \gamma_0 + \Gamma_s \Delta H_{seg} \quad (1)$$

where γ_s is the surface energy of the doped material; γ_0 represents the surface energy of undoped material; Γ_s is the solute excess at the surface; and ΔH_{seg} is the enthalpy of segregation. From Eq. (1), one can draw the conclusion that the surface energies decrease with an increase in the surface excess of the dopant, a concept well established for liquids by Gibbs' adsorption isotherm.

If a dopant is changing the surface energy of an oxide with intrinsic polymorphism, the stability of particular phases can be remarkably affected when the surface area is enlarged (smaller grain sizes). As demonstrated for Y and Ca doped zirconia [25,26], a

* Corresponding author.
E-mail address: rhrcastro@ucdavis.edu (R.H.R. Castro).

http://dx.doi.org/10.1016/j.apsusc.2016.09.126
0169-4332/

new phase diagram complementing the conventional temperature-composition diagram must be introduced, with the grain size as a new key variable to account for the surface energetic contribution. Quantitative prediction of the effect of the dopant on the surface energy is therefore of interest to enable phase stability design.

Many methods have been proposed in the literature to measure the surface energy of oxides [19]. Among them, water adsorption microcalorimetry has recently demonstrated potential to accurately assess surface energies of doped systems [27] and was recently explored in TiO_2 based systems [28]. The principle of this technique is the relationship between the heat of adsorption of water molecules on the surface of the oxide and the surface energy itself. An adsorption theory previously described in details enables calculating the surface energy of the anhydrous surface state or at a given hydration condition [27,29].

In this work, surfaces energies of 0 to 2 mol% Nb_2O_5-doped TiO_2 were measured using water adsorption microcalorimetry [29]. The data was combined with oxide melt drop solution enthalpy to deliver reliable thermodynamic information on the bulk energetics of the system and the results used to build a new, predictive nanophase diagram for anatase-rutile in the studied compositional range.

2. Experimental procedure

2.1. Sample preparation

TiO_2 containing 0, 0.5, 1, 2 and 5 mol% Nb_2O_5 was synthesized by co-precipitation. The samples are labeled in this paper as 0NbTi, 0.5NbTi, 1NbTi, 2NbTi and 5NbTi. The Ti and Nb precursors used were titanium (IV) isopropoxide (TTIP, Aldrich) and niobium butoxide (Aldrich), respectively. TTIP and Nb-butoxide were mixed for 10 min to obtain a homogeneous solution and then dripped into an ammonium hydroxide solution (NH_4OH, 5 M, Fisher Scientific) under vigorous stirring. The obtained colloidal suspension was centrifuged at 3000 rpm for 5 min to separate the nanopowders from the liquid and washed three times (in water, water/ethanol 1:1 in volume, and ethanol) to remove any residual ammonia. The samples were dried at 90 °C for 72 h and ground with a pestle and mortar. In order to obtain anatase phase and eliminate any ethanol residual from the powders, the dried hydroxides were calcined in a box furnace (Lindberg/Blue M) under oxygen atmosphere at 450 °C for 7 h. Bulk rutile phases were obtained after calcination in a tube furnace (Thermolyne type 54500) at 1200 °C for 2 h.

2.2. Characterization

Powder X-ray Diffraction (XRD) patterns were collected using a Bruker AXD D8 Advance diffractometer using Cu$K\alpha$ radiation (λ = 1.5406 Å), operated at 40 kV and 40 mA. Data were collected in the range 20° to 90°. LaB_6 (NIST SRM 660a) was mixed with the samples as a standard for the lattice parameter calculations. The crystallite size was determined by WPF (Whole Pattern Fitting) refinement in the JADE software (version 6.11, 2002, Materials Data Inc., Livermore, CA). Surface area measurements were carried out using the Brunauer, Emmett, and Teller (BET) method with nitrogen gas adsorption (Micromeritics Gemini VII). Thermogravimetry results showed that significant mass changes can only be observed up to 400 °C; hence, this temperature was selected for degassing prior to both BET (Micromeritics VacPrep 061, sample degas system) and water adsorption experiments. Thermal reactions were also investigated by Differential Scanning Calorimetry (DSC, SETSYS Evolution, SETARAM) from room temperature to 1200°C at a heating rate of 10 °C/min.

2.3. Water adsorption

The water adsorption microcalorimetric experiments were performed using a Micromeritics ASAP 2020 coupled with a Calvet-type microcalorimeter (Sensys Evo, Setaram, France). The objective of the experiment is to measure the heat of adsorption of water molecules on the surface of an oxide as a function of the relative pressures. The instrument and methodology are described in detail elsewhere [27,29]. The samples were placed in the chamber and degassed (at 400 °C for 12 h) to ensure an initial anhydrous surface condition. Lightly hand pressed pellets with total surface area ~2 m^2 were used (12–24 mg depending of the sample surface area). The chamber was kept at 25 °C, and the dosing routine was programmed to be ~2 μmol H_2O per dose and equilibration time ~1.75 h for the first four doses, ~1 h for the fifth dose, ~0.75 h for sixth and seventh and ~0.5 h from 8 h on. A correction for water adsorption on the tube and manifold was made from a blank run (empty tubes).

The anhydrous surfaces energies of the synthesized specimens were calculated using the water adsorption data and computing them using a custom written function (MATLAB Release 2010a, MathWorks, Natick, MA), reported elsewhere [29]. The water adsorption curve was fitted using a modified Langmuir-BET adsorption curve (Eq. (2)), where the regression equation fit the water adsorption data as a function of pressure;

$$\theta = \theta_c \frac{b\sqrt{x}}{1+b\sqrt{x}} + \theta_p \frac{cx}{(1-x)(1+(c-1)x)} \quad (2)$$

where $\theta_c$is the monolayer coverage of the dissociative water; θ_p is the physisorption monolayer coverage; b and c are unit-less fit parameters that depend on the specimen; and x is the relative pressure (p/p_0). The differential heat of adsorption curve was fitted using Eq. (3) [29].

$$\frac{dH_R}{d\theta} = De^{-\theta/d} + E\left(f\theta - \theta^2\right)e^{-\theta/e} + \frac{dH_{con}}{d\theta}\Big|_{T_{o,p_o}} \quad (3)$$

Eq. (3) is an empirical relationship for the differential heat of water adsorption as a function of the water coverage, where H_R is the heat of adsorption, and H_{con} is the enthalpy of liquefaction of water. The equation requires five parameters: d and e are decay parameters that relate how strong the specimen's surface affects the adsorbed water; and D, E, and f are fit parameters with units of kJ/mol, kJ/mol^3, and mol, respectively.

After fitting the water adsorption curve and the differential heat of adsorption data using Eqs. (2) and (3), the surfaces energies of the samples were numerically computed by plugging the mentioned equations into Eq. (4).

$$SA\frac{d^2\gamma}{dx^2} = \frac{d\theta}{dx}\left\{\frac{d^2H_r}{d\theta^2}\frac{d\theta}{dx} + \frac{d\mu_{gas}}{dx} - \gamma\frac{d^2SA}{d\theta^2}\frac{d\theta}{dx} + \frac{d\gamma}{dx}\left(\frac{SA}{\theta} - 2\frac{dSA}{d\theta} + SA\frac{d^2\theta}{dx^2}\left(\frac{dx}{d\theta}\right)^2\right)\right\} \quad (4)$$

Eq. (4) correlates the surface energy and water adsorption. The adsorbed water is a function of the pressure, x; and the differential heat of water adsorption is a function of the adsorbed water, θ. In this Equation, SA is the surface area of the sample; γ is the surface energy at a given state; and μ_{gas} is the vapor chemical potential.

2.4. Oxide melt solution calorimetry

High-temperature drop solution calorimetry was carried out using a custom-built Calvet-type twin calorimeter [30]. This equipment provides energy of dissolution of oxide samples, which

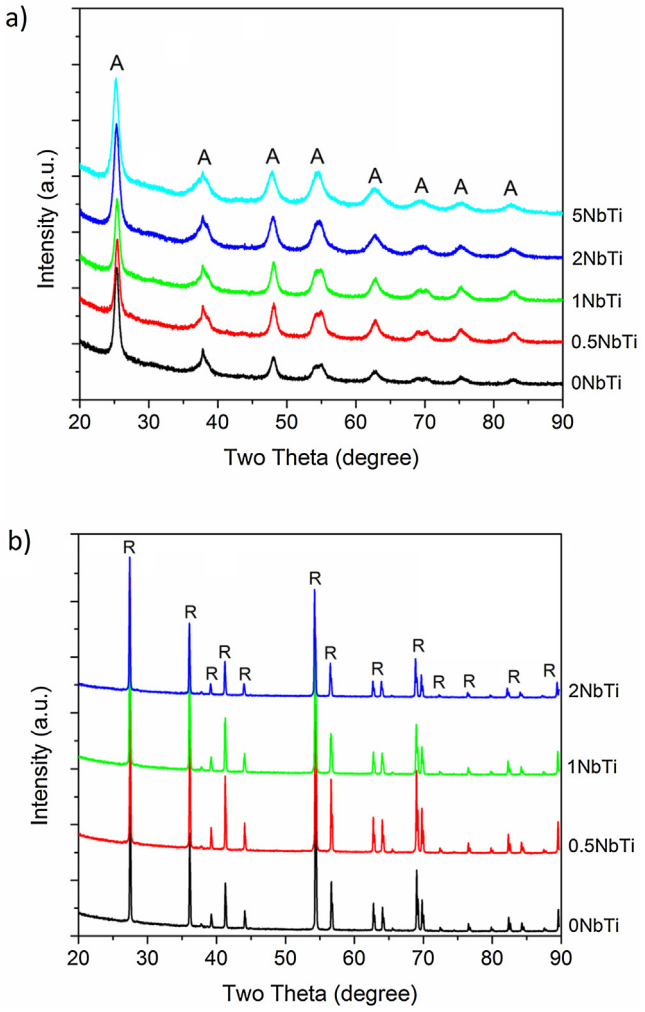

Fig. 1. XRD patterns of Nb_2O_5-doped TiO_2. a) Anatase (0–5 mol%), and b) Rutile (0–2 mol%).

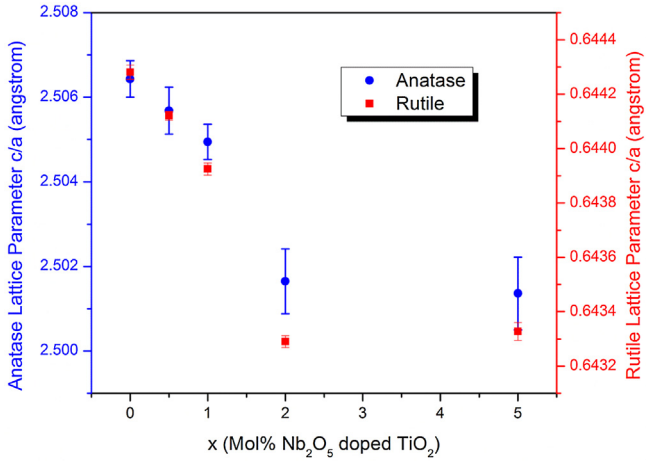

Fig. 2. The lattice parameter ratio (c/a) for 0–5 mol% Nb_2O_5-doped-TiO_2 samples for anatase and rutile phases.

appropriate thermochemical cycles can be used to obtain bulk enthalpy information. Laboratory standard calibration with transposed temperature drops of ~5 mg alpha alumina pellets was used. Hand pressed pellets (~5 mg) were weighted using microbalance and dropped into molten sodium molybdate ($3Na_2O{\cdot}4MoO_3$) solvent at ~800 °C in the calorimeter. Oxygen was bubbled through the solvent at the rate of 3.3 mL/min to facilitate sample dissolution. Oxygen was also flushed over the solvent in the calorimeter (50 mL/min) to maintain constant composition for the gas phase over solvent. Changes in the composition of the gas above the solvent can change the heat flow characteristics of the calorimeter during an experiment. Before dropping the samples in the calorimeter, the powders were left in the calorimetric suite for at least 3 days to equilibrate in a 50% relative humidity environment. Several drops were made to obtain statistics. The error reported was determined by the standard deviations. Thermogravimetry was used to measure the water content on the samples at degassing conditions to enable a quantitative thermochemical cycle.

3. Results and discussion

3.1. Nanoparticles' characterization

The X-ray diffraction patterns for pure TiO_2 and Nb_2O_5-doped TiO_2 samples are shown in Fig. 1. The pure (undoped) anatase phase (JCPDS card n. 71–1167) used in the experiments is shown in Fig. 1a. Broad peaks can be observed, which is typical of nanosized crystallites. No second phase was detected by XRD, so that only the peaks referred to the anatase phase are indicated. The absence of niobium oxide phases suggests that niobium is dissolved into TiO_2 or segregated at the surface of titania nanoparticles. The powders referring to the rutile phase were calcined at 1200 °C for 2 h and are shown in Fig. 1b. The polymorph is referenced using JCPDS card n.86-0147. Sharp peaks are observed, which is common in bulk samples. Notice that the diffraction pattern for 5 mol% Nb_2O_5-doped TiO_2 is not shown at Fig. 1b. This sample has presented titanium niobium oxide phase ($TiNb_2O_7$–monoclinic, JCPDS card n. 39–1407) in addition to rutile [18]. Thus, the energetic studies, which requires single phase were not carried out for this sample. No second phase was detected for 0–2 mol% Nb_2O_5-doped-TiO_2 rutile. All peaks match with TiO_2 rutile phase.

The results for lattice parameters a, b and c for both anatase and rutile phases are shown in Table 1. A systematic expansion is observed in the lattice parameters with increasing of Nb_2O_5 doping. As the ionic radius of the Nb^{5+} ions into octahedral coordination is larger than Ti^{4+}, the increase in the cell parameters with the increasing Nb content confirms that Nb is incorporated in the TiO_2 lattice. This trend is in agreement with the results found in the literature [4,17]. The lattice parameter ratio (c/a) for anatase and rutile phases is shown in Fig. 2. Both phases have similar trend. Up to 2 mol% Nb_2O_5 doping, a systematic decreasing on the c/a ratio is observed, and for 5 mol% the value is statistically the same as 2 mol% Nb_2O_5-doping. The ratio decreasing with the increasing Nb_2O_5 concentration suggests the formation of limited solid solution. In this work, the limit was achieved at 2 mol% Nb_2O_5-doping (samples with 5 mol% were observed to show second phase). Thus, this value was used as doping limit for surface energies and enthalpy of drop solution measurements. Consequently, it was chosen as the doping limit for the phase diagram as well. According to Vegard's law [31], a linear dependence of lattice parameter on dopant concentration is expected when all dopant content is dissolved in solid solution. The deviation from linearity proposes the occurrence of surface segregation [20].

The grain sizes calculated from WPF refinement for all samples are shown in Table 1. For anatase phase it is possible to observe a systematic decreasing in the grain sizes as the doping content increases. As all anatase samples were calcined at the same temperature and time, the decrease on the grain sizes can be attributed to Nb_2O_5-doping content, which suggests an increase in the stability of TiO_2 nanoparticles against coarsening. According to coarsening models [32], the particle size is directly proportional to the surface

Table 1
Grain sizes and lattice parameters calculated using a WPF Refinement in JADE 6 Software. The oxide melt drop solution enthalpies are tabulated for both the as measured drop solution experiments (ΔH_{DS}) and as bulk corrected enthalpies (ΔH_{Bulk}). The number in parentheses denotes the number of drops reported in the average value and used to determine the standard errors.

Sample	*Grain size (nm)*	*Lattice Parameter a = b (Å)*	*Lattice Parameter c (Å)*	*Enthalpy of drop solution ΔH_{DS} (kJ/mol)*	*Bulk enthalpy of drop solution ΔH_{Bulk} (kJ/mol)*
0NbTi (Anatase)	11.8 ± 0.3	3.78732 ± 0.00026	9.49265 ± 0.00098	75.08 ± 0.56(6)	63.90 ± 0.69(6)
0.5NbTi (Anatase)	9.6 ± 0.3	3.78869 ± 0.00030	9.49325 ± 0.00134	76.19 ± 0.96(7)	65.75 ± 1.06(7)
1NbTi (Anatase)	8.4 ± 0.2	3.79022 ± 0.00029	9.49428 ± 0.00097	78.43 ± 0.58(7)	67.73 ± 0.97(7)
2NbTi (Anatase)	6.8 ± 0.2	3.79422 ± 0.00044	9.49179 ± 0.00179	80.29 ± 0.36(7)	65.17 ± 0.76(7)
5NbTi (Anatase)	5.9 ± 0.3	3.79924 ± 0.00054	9.50327 ± 0.00190	–	–
0NbTi (Rutile)	>100	4.59256 ± 0.00009	2.95890 ± 0.00006	73.92 ± 0.77(11)	73.92 ± 0.77(11)
0.5NbTi (Rutile)	>100	4.59448 ± 0.00005	2.95940 ± 0.00004	73.59 ± 0.77(10)	73.59 ± 0.77(10)
1NbTi (Rutile)	>100	4.59732 ± 0.00008	2.96033 ± 0.00005	74.86 ± 0.79(10)	74.86 ± 0.79(10)
2NbTi (Rutile)	>100	4.60321 ± 0.00007	2.96120 ± 0.00005	72.54 ± 0.76(12)	72.54 ± 0.76(12)
5NbTi (Rutile)	>100	4.60330 ± 0.00011	2.96143 ± 0.00008	–	–

energy, then it is expected that a decreasing surface energy promotes smaller particle sizes at a given temperature. The grain sizes for rutile phases are >100 nm, so the WPF refinement cannot give a reliable result for grain size.

3.2. Surface energy measurements

The surface energies of the polymorphs were determined using water adsorption microcalorimetry. Fig. 3 shows the isotherm curves for anatase phase. Enthalpy of adsorption plotted against water coverage is shown in Fig. 3a and water coverage *versus* relative pressure in Fig. 3b. According to Castro and Quach [27], the adsorption behavior shows the presence of three stages based on the derivative of the adsorption isotherm curve. At very small relative pressures (<0.02), there is a rapid increasing on coverage when the pressure increases. The enthalpies of water adsorption in this first stage are very negative, suggesting a highly reactive surface. These exceedingly negative heats at low coverage indicate that there is a strong exothermic reaction in the first few monolayers. This can be explained by the dissociative nature of water due to chemisorbed water bonds with the surface [29]. For the second stage, which is up to about 0.3, the slope of the isotherm is smaller. In addition, at the third region (relative pressure>0.3), the slope of the isotherm curve rapidly increases. However, the differential enthalpy of water adsorption gets close to the enthalpy of liquid water condensation, −44 kJ/mol (dotted line at Fig. 3a), indicating that the new adsorbed water layers present a liquid-like behavior [27].

In order to calculate the surface energy, one should fit the data using Eqs. (2) and (3), followed by solving differential Eq. (4). Fig. 4 shows the surface energies values for 0–2 mol% Nb_2O_5-doped-TiO_2 *versus* surface area. The surface energies and surface area are inversely proportional. The surface energy for the anatase phase decreases while the surface area increases as a function of the Nb concentration. This is consistent with the crystallite size data, and confirms an increase in the thermodynamic stability of the nanoparticles with decreasing surface energy [24]. This phenomenon can also be associated to surface segregation of dopants. As the Nb_2O_5 has a potential to segregate on the surface of TiO_2 under oxidizing conditions [18], the decreasing on surface energy and increasing on the surface area is expected. In addition to the thermodynamics, though, the segregated dopant, niobium pentoxide on the surface of TiO_2, can also act as pinning agent limiting the growth rate. This behavior has been also observed for chromium-doped SnO_2, an iso-structural material [33].

Table 2 compares the surface energies from this work to the literature data for undoped TiO_2 (Nb_2O_5-doped-TiO_2 surface energies are not available for comparison). The TiO_2 anatase surface energy found in this work was 0.95 ± 0.03 J/m^2. The results calculated with DFT by Hummer *et al.* [4] and Lazzeri et al. [6] for (001)

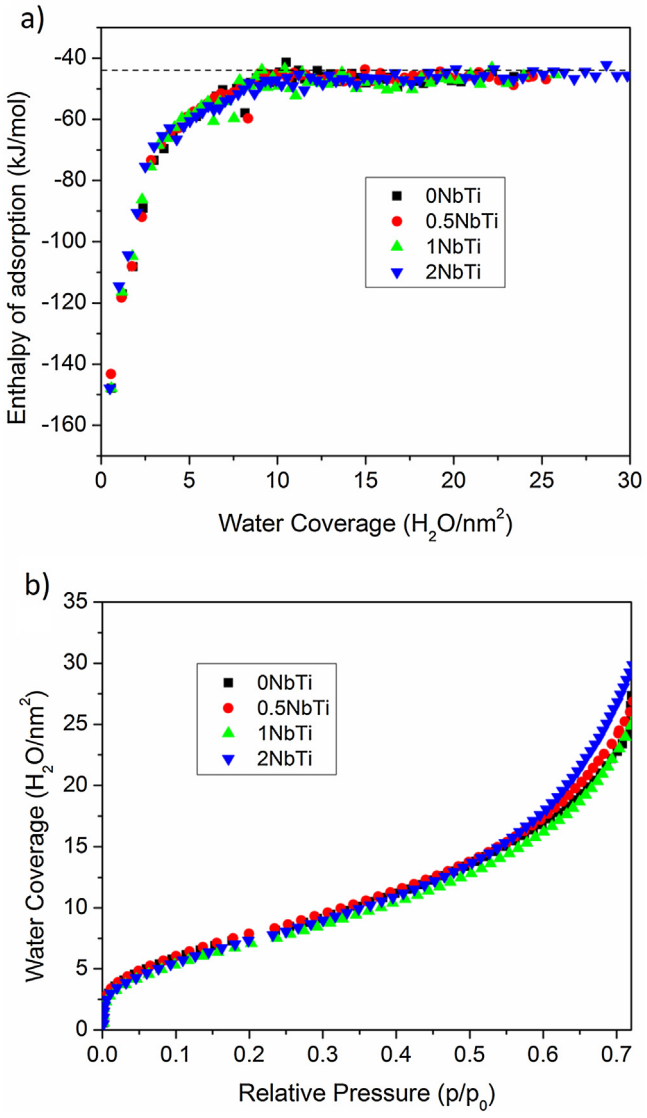

Fig. 3. Water adsorption microcalorimetry data: (a) Enthalpy of water adsorption plotted against water coverage; (b) Water coverage isotherms plotted as H_2O molecules per nm^2 against the relative pressure.

plane are 0.96 and 0.90 J/m^2, respectively. These results are pretty consistent to the value shown in this work for undoped anatase titania. However, the values are not in agreement with simulations for other planes (100), (101) and (110) reported by Barnard and Zapol [7]. This is not contradictory, though, as in fact our experi-

Table 2
Surface energies for anatase TiO_2 (J/m^2) as measured by water adsorption microcalorimetry and from literature data as indicated.

Castro and Wang [8]	Levchenko et al. [2]	Hummer et al. [4]	Lazzeri et al. [5,6]	Barnard and Zapol [7]	Naicker et al. [3]	This work
0.67 ± 0.05	0.74 ± 0.04	0.96 (001) 0.51 (100) 0.41 (101)	0.90 (001) 1.09 (110) 0.44 (101)	0.51 (001) 0.81 (110) 0.35 (101)	2.1	0.95 ± 0.03 (0NbTi) 0.87 ± 0.03 (0.5NbTi) 0.88 ± 0.03 (1NbTi) 0.78 ± 0.02 (2NbTi)

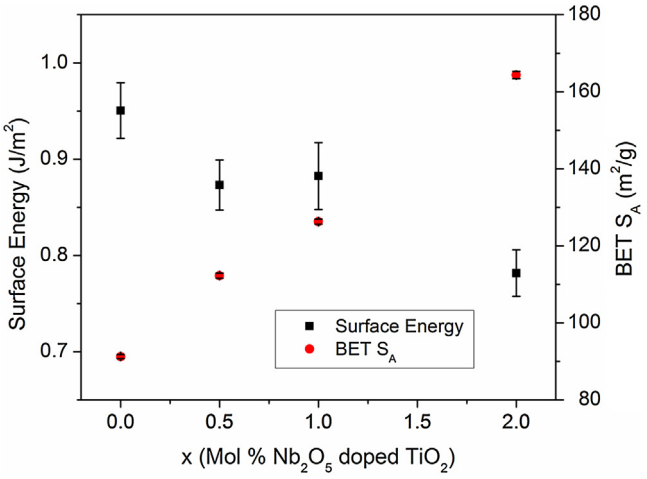

Fig. 4. Surface energy (J/m^2) versus BET surface area (m^2/g) is plotted against 0–2 mol% of Nb_2O_5-doped-TiO_2 (anatase phase).

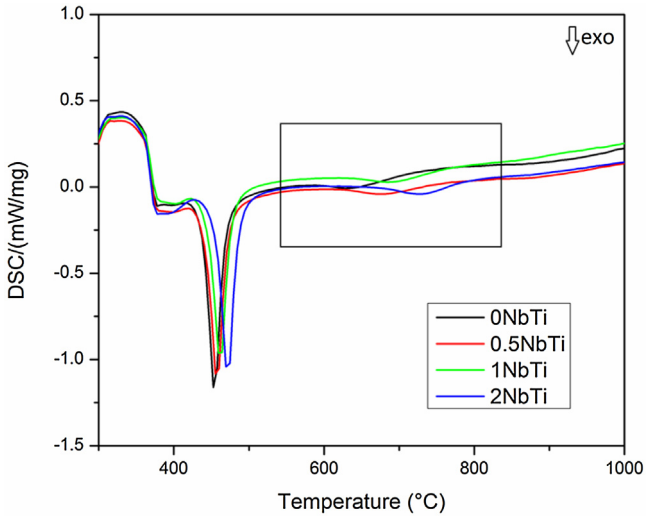

Fig. 5. Differential scanning calorimetry (DSC) from from 300 to 1000 °C.

mental surface energy is a result of averaging of the contribution of all present surface planes. Naicker *et al.* [3] have found a surface energy of 2.1 J/m^2 by using molecular dynamics in whole nanoparticles (where surface planes are averaged like in our experimental work). This value is however very high, what can be explained by the fact their particles are too small (<4 nm). Small particles have non-negligible energetic effects of edges, defects, and high-index, high-energy surfaces effects on the total surface energy. As the particle size increases, the effect of edges and defects is expected to decrease [4]. Castro and Wang [8], and Levchenko *et al.* [2] have presented experimental data on anatase surface energy for pure TiO_2 to be 0.67 ± 0.05 and 0.74 ± 0.04 J/m^2, respectively. These are lower than ours, but the TiO_2 particles were synthesized hydrothermally by these researchers. The synthesis method is well known to have effects on morphology of the particles and hence on average surface energies.

Due to limitations of the water adsorption microcalorimetry technique on measuring coarsened samples, we were not able to directly determine the surface energy of rutile polymorphs. For the phase stability analysis, the rutile surface energy was assumed as 2.2 ± 0.07 J/m^2 based on recent calorimetric experiments [2].

Fig. 5 shows the differential scanning calorimetry data for 0–2 mol% Nb_2O_5-doped TiO_2 from from 300 to 1000 °C. A first large exothermic peak is attributed to the crystallization, transformation from amorphous to anatase phase [34]. The second smaller exothermic peak observed between 600 and 800 °C is attributed to the anatase-rutile phase transition. It is clearly observed that the peaks move to the right side of the graph as the doping percentage increases. This shift shows that Nb_2O_5-doping is postponing the anatase-rutile phase transition in ~150 °C, suggesting that the doped samples are more stable than undoped samples. These results agree with the increase in stability of the anatase polymorph evidenced by surface energy, surface area and grain sizes data.

3.3. Bulk energy measurements

Data on bulk energetics of each polymorph and composition are required to build a complete stability diagram. The bulk enthalpy can be related to its heat of "drop solution" measured by oxide melt drop solution calorimetry. The experiment is explained in detail in the experimental section. The samples were dropped from room temperature into a molten melt of sodium molybdate maintained at ~800 °C and the enthalpy of drop solution was recorded after complete dissolution. Taking the differences in heat of drop solution of each phase, it is possible to determine the enthalpy difference during phase transition. In order to remove any surface contribution from the dissolution process and extract bulk enthalpy data, the rutile phase was calcined at 1200 °C for 2 h. On the other hand, since anatase could not be coarsened under the risk of transforming to rutile, the anatase data were corrected for adsorbed water and surface energy effects using the water adsorption data and heat content of H_2O vapor between 25 and 800 °C as 29.05 kJ/mol (see Ref. [24] for details on drop solution corrections).

Table 1 shows the uncorrected and corrected enthalpy of drop solution (ΔH_{ds}) measured for rutile and anatase phases of TiO_2 and Nb_2O_5-doped TiO_2. The differences among ΔH_{ds} for undoped TiO_2 rutile and doped samples are very small, but one observes that the uncorrected ΔH_{ds} tends to be less endothermic with the increasing of Nb_2O_5 concentration, while the surface-corrected ΔH_{ds} for bulk anatase shows negligible variance. This behavior confirms that Nb_2O_5-doping is stabilizing the anatase phase by decreasing its surface energy. According to the data presented in Table 1, the bulk-enthalpy of phase transition of TiO_2 is 10.02 ± 0.74 kJ/mol. The data

found in the literature have a significant variation. Ranade et al. [35] have reported rutile-anatase enthalpy of transformation for TiO_2 being 2.61 ± 0.41 kJ/mol. Navrotsky and Kleppa [36], have obtained the enthalpy of phase transformation at 968 K as 6.57 ± 0.79 kJ/mol. They have used high-temperature oxide melt solution calorimetry in both cases [35,36]. Hummer et al. [4] suggested that the transition enthalpy for the nanoanatase to nanorutile transition is 3.5, 6.8, and 2.5 kJ/mol for 1, 2, and 3 nm particles, respectively. They reported that the contribution of edges and vertices to the total surface energy decreases with particle size, while the change in the contribution from 2D surface structure is more modest. As a consequence, if edge and corner energies were not taken in consideration, the total transition enthalpy for nanoanatase to nanorutile would become 25.3, 11.9, and 13.2 kJ/mol for 1, 2, and 3 nm particles, respectively [4].

The final data necessary to complete the nanophase diagram are entropy values, which require C_p measurements from zero absolute to room temperature. In this case, Drazin and Castro [26] have suggested the use of surface energy, bulk enthalpy, and entropy data to create the diagram for the surface area and grain size critical for the phase transformation. According to their work, a standard surface excess term is generally added to the Gibbs free energy to account for the increased surface area (Eq. (5)).

$$G = H - TS + SA\gamma \tag{5}$$

where H is the molar enthalpy in kJ/mol; T is the absolute temperature in K; S is the molar entropy in J/mol; SA is the surface area in m^2/mol; and γ is the surface energy in J/m^2.

The Gibbs free energy should be zero at chemical equilibrium between any two α and β polymorphs. Considering that the reaction occurs via a constant surface area process, we can write Eq. (6), where the delta symbol corresponds to the difference in the appropriate quantity of α and β polymorphs.

$$\Delta G_{\alpha\to\beta} = \Delta H_{\alpha\to\beta} - T\Delta S_{\alpha\to\beta} + SA \cdot \Delta\gamma_{\alpha\to\beta} = 0 \tag{6}$$

The surface area of transition can be solved rearranging Eq. (6) as shown in Eq. (7). In order to the transformation happens naturally the denominator and numerator have to be positive simultaneously.

$$SA = \frac{\left(H_\beta - H_\alpha\right) - T\cdot\left(S_\beta - S_\alpha\right)}{\left(\gamma_\beta - \gamma_\alpha\right)} \tag{7}$$

The entropies for anatase and rutile are reported in the literature and have similar values [S^0 (298 K, rutile) = 50.35 ± 0.1 J/mol · K and S^0 (298 K, anatase) = 49.79 ± 0.1 J/mol · K] [37]. Nevertheless, $T\Delta S$ was included in the calculations, but it did not change the overall sequence of stability. We assume here that entropic contributions for the small Nb doping are negligible.

3.4. Stability crossover and composition dependence

The nanophase diagram for Nb_2O_5-doped-TiO_2 is shown in Fig. 6. The stability crossover between the two polymorphs was calculated in m^2/mol. However, the grain size is a more prevalent parameter. Thus, the surface area crossover was converted to grain size using the molar mass and density of Nb-Ti in conjunction with an approximation for the ideal specific surface area of a circular particle using Eq. (8).

$$SA\left(\frac{m^2}{g}\right) = \frac{6}{\rho d} \tag{8}$$

where SA is the surface area; ρ is the density; and d is the grain size [26].

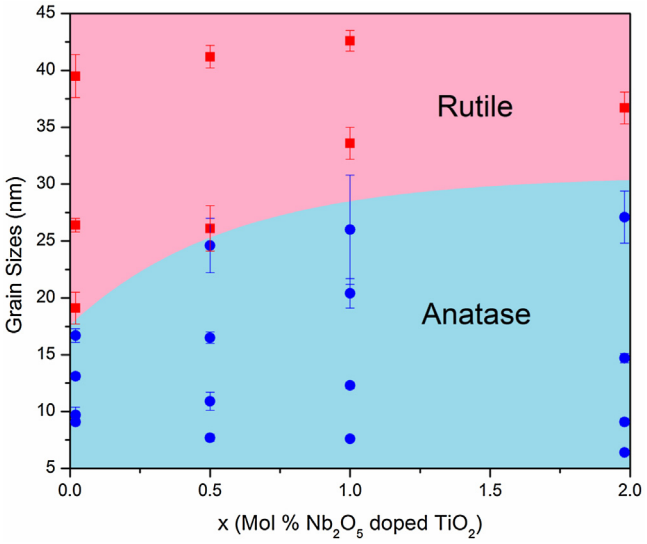

Fig. 6. Grain size nanophase diagram. The shaded regions show the stable titania polymorph given a grain size in nm and Nb_2O_5 content in mol percent. The color coding is light red for rutile phase and light blue for anatase phase. Red square points are rutile phase obtained from real samples and grain sizes calculated using a WPF Refinement in JADE 6 Software. Blue dots are anatase phase real samples with grain sizes calculated using a WPF Refinement in JADE 6 Software. (For interpretation of the references to colour in this figure legend, the reader is referred to the web version of this article.)

The calculated crossover between the two polymorphs in function of Nb_2O_5-concentration was fitted using the exponential Eq. (9).

$$y = y_0 + 13.13686 \times \left(1 - e^{-\frac{x}{0.568}}\right) \tag{9}$$

where y is the crossover grain size; y_0 is the crossover for undoped TiO_2, which is 17.6 nm for this work; and x is the Nb_2O_5 molar fraction.

The shaded regions show the stable TiO_2 polymorph given a grain size in nm and Nb_2O_5 content in mole percent. According to the nanocrystalline phase diagram, Nb_2O_5-doping allows the TiO_2 to grow more in anatase phase before it transforms into rutile. The shape of the curve is similar to the inverse trend of surface energy against doping content. Therefore, we attribute the anatase stability according to the Nb concentration to the decreasing in surface energy.

Experimental data were collected to verify the veracity of the diagram. Samples were intentionally calcined to achieve specific grain sizes and the phases analyzed by X-ray diffraction. The results are shown in Fig. 6 as red squares for rutile phase and blue circles for anatase. These experimental results fit well with the proposed nanocrystalline diagram, confirming that the energetic analysis is quite predictive with respect to the phase stability.

The anatase-rutile crossover has been studied for undoped TiO_2 by several researches and the critical transformation values vary considerably. Barnard and Zapol [7], using density functional calculations, have found the anatase-rutile phase transition to be ~9.3 nm. They also reported that the transition energy and size vary depending upon factors such as reaction atmosphere and synthesis conditions. The anatase-to-rutile phase transition size also depends on the surface passivation. The size increases significantly to 23.1 nm when both the bridging oxygen and under-coordinated titanium atoms of the surface trilayer are H-terminated. Zhang and Banfield [38], assuming the surface stress equals the surface free energy in value, have reported that anatase is more stable than rutile for particle sizes lower than 14 nm, and lower than 9 nm if

surface stress is not considered. Li et al., [39] using sol gel synthesis, have suggested the critical size for transition of anatase to rutile in somewhere between 32 and 42 nm. Castro and Wang [8], and Levchenko et al., [2] have reported the critical size for free nanoparticles as 61 and 67 nm, respectively. According to this short literature survey, this interval (9–67 nm) can be affected by the synthesis method, particle morphology, surface stress and purity. Our data fit within this, as it is a very broad range. Regardless of agreement with literature, our experimental results demonstrate that the thermodynamics of nanosized TiO_2 and the effect of dopants can significantly affect the polymorphism. In a particular set of samples, the thermodynamic data can be used to predict polymorphism.

4. Conclusions

A predictive anatase-rutile phase transition diagram was built at nanoscale for Nb_2O_5-doped-TiO_2. Nb_2O_5-doping postpones the ART, allowing the anatase grains to grow more than undoped TiO_2 before phase transition is observed. The stability crossover for undoped TiO_2 was found to be 17.3 nm, while 2 mol% Nb_2O_5-doped-TiO_2 crossover is ~30 nm. The nanophase diagram agrees with the experimental data used in this work. The surface energy for Nb_2O_5-doped-TiO_2 decreases systematically as the Nb concentration increases, confirming the higher stability for doped samples. This result is a powerful predictive tool that can be applied for nanotechnological efforts on Nb-Ti oxide systems.

Acknowledgments

AS and DH gratefully acknowledge the Brazilian funding agencies CAPES (Process no. 11217/13-8) and CNPq (Process no. 216202/2014-0). RC acknowledges National Science Foundation DMR 1055504 and UC Lab Fees Research Program 12-LF-239032.

References

[1] M. Pelaez, N.T. Nolan, S.C. Pillai, M.K. Seery, P. Falaras, A.G. Kontos, P.S.M. Dunlop, J.W.J. Hamilton, J.A. Byrne, K. O'shea, M.H. Entezari, D.D. Dionysiou, A review on the visible light active titanium dioxide photocatalysts for environmental applications, Appl. Catal. B 125 (2012) 331–349.
[2] A.A. Levchenko, G. Li, J. Boerio-Goates, B.F. Woodfield, A. Navrotsky, TiO_2 stability landscape: polymorphism, surface energy, and bound water energetics, Chem. Mater. 18 (2006) 6324–6332.
[3] P.K. Naicker, P.T. Cummings, H. Zhang, J.F. Banfield, Characterization of titanium dioxide nanoparticles using molecular dynamics simulations, J. Phys. Chem. B 109 (2005) 15243–15249.
[4] D.R. Hummer, J.D. Kubicki, P.R.C. Kent, J.E. Post, P.J. Heaney, Origin of nanoscale phase stability reversals in titanium oxide polymorphs, J. Phys. Chem. C 113 (2009) 4240–4245.
[5] M. Lazzeri, A. Vittadini, A. Selloni, Erratum: structure and energetics of stoichiometric TiO_2 anatase surfaces, Phys. Rev. B 65 (2002) 119901.
[6] M. Lazzeri, A. Vittadini, A. Selloni, Structure and energetics of stoichiometric TiO_2 anatase surfaces, Phys. Rev. B 63 (2001) 155409.
[7] A.S. Barnard, P. Zapol, Effects of particles morphology and surface hydrogenation on the phase stability of TiO_2, Phys. Rev. B 70 (2004) 235403.
[8] R.H.R. Castro, B. Wang, The hidden effect of interface energies in the polymorphic stability of nanocrystalline titanium dioxide, J. Am. Ceram. Soc. 94 (2011) 918–924.
[9] L. Gan, C. Wu, Y. Tan, B. Chi, J. Pu, L. Jian, Oxygen sensing performance of Nb-doped TiO_2 thin film with porous structure, J. Alloys Compd. 585 (2014) 729–733.
[10] R.K. Sharma, M.C. Bhatnagar, G.L. Sharma, Effect of Nb metal ion in TiO_2 oxygen gas sensor, Appl. Surf. Sci. 92 (1996) 647–650.
[11] W. Zeng, T. Liu, Z. Wang, Impact of Nb doping on gas-sensing performance of TiO_2 thick-film sensors, Sensor Actuat. B-Chem. 166–167 (2012) 141–149.
[12] S.G. Kim, M.J. Ju, I.T. Choi, W.S. Choi, H.J. Choi, J.B. Baek, H.K. Kim, Nb-doped TiO_2 nanoparticles for organic dye-sensitized solar cells, RSC Adv. 3 (2013) 16380–16386.
[13] M.K. Siddiki, D. Munoz-Rojas, J. Oro, J.J. Li, Q. Qiao, D.W. Galipeau, M. Lira-Cantu, Synthesis and characterization of Nb doped titania for dye sensitized solar cells, IEEE Photovolt. Spec. Conf., 34th (2009) 685–689.
[14] C.R. Estrellan, C. Salim, H. Hinode, Photocatalytic decomposition of perfluorooctanoic acid by iron and niobium co-doped titanium dioxide, J. Hazard. Mater. 179 (2010) 79–83.
[15] A.L. Castro, M.R. Nunes, M.D. Carvalho, L.P. Ferreira, J.C. Jumas, F.M. Costa, M.H. Florêncio, Doped titanium dioxide nanocrystalline powders with high photocatalytic activity, J. Solid State Chem. 182 (2009) 1838–1845.
[16] A.L. da Silva, D.N.F. Muche, S. Dey, D. Hotza, R.H.R. Castro, Photocatalytic Nb_2O_5-doped TiO_2 nanoparticles for glazed ceramic tiles, Ceram. Int. 42 (2016) 5113–5122.
[17] A.M. Ruiz, G. Dezanneau, J. Arbiol, A. Cornet, J.R. Morante, Insights into the structural and chemical modifications of Nb additive on TiO_2 nanoparticles, Chem. Mat. 16 (2004) 862–871.
[18] A.J. Atanacio, T. Bak, J. Nowotny, Niobium segregation in niobium-doped titanium dioxide (Rutile), J. Phys. Chem. C 118 (2014) 11174–11185.
[19] R.H.R. Castro, On the thermodynamic stability of nanocrystalline ceramics, Mater. Lett. 96 (2013) 45–56.
[20] D. Gouvêa, G.J. Pereira, L. Gengembre, M.C. Steil, P. Roussel, A. Rubbens, P. Hidalgo, R.H.R. Castro, Quantification of MgO surface excess on the SnO_2 nanoparticles and relationship with nanostability and growth, Appl. Surf. Sci. 257 (2011) 4219–4226.
[21] M.J. Godinho, R.F. Gonçalves, L.P.S. Santos, J.A. Varela, E. Longo, E.R. Leite, Room temperature co-precipitation of nanocrystalline CeO_2 and $Ce_{0.8}Gd_{0.2}O_{1.9-\delta}$ powder, Mater. Lett. 61 (2007) 1904–1907.
[22] R.H.R. Castro, S.V. Ushakov, L. Gengembre, D. Gouvêa, A. Navrotsky, Surface energy and thermodynamic stability of (-alumina: effect of dopants and water, Chem. Mater. 18 (2006) 1867–1872.
[23] L. Wu, S. Dey, M. Gong, F. Liu, R.H.R. Castro, Surface segregation on manganese doped ceria nanoparticles and relationship with nanostability, J. Phys. Chem. C 118 (2014) 30187–30196.
[24] C.H. Chang, M. Gong, S. Dey, F. Liu, R.H.R. Castro, Thermodynamic stability of SnO_2 nanoparticles: the role of interface energies and dopants, J. Phys. Chem. C 119 (2015) 6389–6397.
[25] J.W. Drazin, R.H.R. Castro, Phase stability in calcia-doped zirconia nanocrystals, J. Am. Ceram. Soc. 99 (2016) 1778–1785.
[26] J.W. Drazin, R.H.R. Castro, Phase stability in nanocrystals: a predictive diagram for yttria-zirconia, J. Am. Ceram. Soc. 98 (2015) 1377–1384.
[27] R.H.R. Castro, D.V. Quach, Analysis of anhydrous and hydrated surface energies of gamma Al_2O_3 by water adsorption microcalorimetry, J. Phys. Chem. C 116 (2012) 24726–24733.
[28] J. Miagava, A.L. da Silva, A. Navrotsky, R.H.R. Castro, D. Gouvêa, The nanocrystalline SnO_2-TiO_2 system part II: surface energies and thermodynamic stability, J. Am. Ceram. Soc. 99 (2016) 638–644.
[29] J.W. Drazin, R.H.R. Castro, Water adsorption microcalorimetry model: deciphering surface energies and water chemical potentials of nanocrystalline oxides, J. Phys. Chem. C 118 (2014) 10131–10142.
[30] A. Navrotsky, Progress and new directions in high temperature calorimetry revisted, Phys. Chem. Miner. 24 (1997) 222–241.
[31] A.R. Denton, N.W. Ashcroft, Vegard's law, Phys. Rev. A 43 (1991) 3161–3164.
[32] R.H.R. Castro, Overview of conventional sintering, in sintering: mechanisms of conventional nanodensification and field assisted processes (Engineering materials), in: R.H.R. Castro, K. van Benthem (Eds.), Sintering Mechanisms of Convention Nanodensification and Field Assisted Processes, Springer-Verlag Berlin Heidelberg, New York, 2013, pp. 17–34.
[33] R.H.R. Castro, J. Rufner, P. Hidalgo, D. Gouvêa, J.A.H. Coaquira, K.V. Benthem, Surface segregation in chromium-doped nanocrystalline tin dioxide pigments, J. Am. Ceram. Soc. 95 (2012) 170–176.
[34] N. Ahmadi, A. Nemati, M. Solati-Hashjin, Synthesis and characterization of co-doped TiO_2 thin films on glass-ceramic, Mater. Sci. Semicond. Process. 26 (2014) 41–48.
[35] M.R. Ranade, A. Navrotsky, H.Z. Zhang, J.F. Banfield, S.H. Elder, A. Zaban, P.H. Borse, S.K. Kulkarni, G.S. Doran, H.J. Whitfield, Energetics of nanocrystalline TiO_2, Proc. Natl. Acad. Sci. U. S. A. 99 (2002) 6476–6481.
[36] A. Navrotsky, O.J. Kleppa, Enthalpy of the anatase-rutile transformation, J. Am. Ceram. Soc. 50 (1967) 626.
[37] S.J. Smith, R. Stevens, S. Liu, G. Li, A. Navrotsky, J. Boerio-Goates, B.F. Woodfield, Am. Miner. 94 (2009) 236–243.
[38] H. Zhang, J.F. Banfield, Thermodynamic analysis of phase stability of nanocrystalline titania, J. Mat. Chem. 8 (1998) 2073–2076.
[39] G. Li, L. Li, J. Boerio-Goates, High purity anatase TiO_2 nanocrystals: near room-temperature synthesis, grain growth kinetics, and surface hydration chemistry, J. Am. Ceram. Soc. 127 (2005) 8659–8666.